Journal of Colloid and Interface Science 440 (2015) 253–262

Contents lists available at ScienceDirect

Journal of Colloid and Interface Science

www.elsevier.com/locate/jcis

Arsenate adsorption onto Fe-TNTs prepared by a novel water–ethanol hydrothermal method: Mechanism and synergistic effect

Yanqi Wang [a,b], Wen Liu [b], Ting Wang [a,b], Jinren Ni [b,*]

[a] State Key Laboratory of Soil Erosion and Dryland Farming on the Loess Plateau, Institute of Water and Soil Conservation, Chinese Academy of Sciences and Ministry of Water Resources, Yangling, 712100 Shaanxi, P.R. China
[b] The Key Laboratory of Water and Sediment Sciences, Ministry of Education, Department of Environmental Engineering, Peking University, Beijing 100871, China

ARTICLE INFO

Article history:
Received 14 April 2014
Accepted 21 October 2014
Available online 4 November 2014

Keywords:
Fe-TNTs
Synergistic effect
Arsenate
Complexation
Two-site Langmuir

ABSTRACT

Arsenate adsorption onto Fe_2O_3 was highly restricted at acidic condition due to dramatic dissolution. To overcome this difficulty, iron oxide nanoparticle-grafted titanate nanotubes (Fe-TNTs) were synthesized by a facile one-step water–ethanol hydrothermal method and used to remove As(V) from aqueous solutions. This new adsorbent was acid-resistant, and showed a large As(V) adsorption capacity of 90.96 mg/g determined by two-site Langmuir model, which was almost 3 times of the original TNTs. Fe_2O_3 was proved to bonded to the surface of TNTs by TEM and XRD analysis and synergy of Fe_2O_3 and TNTs was of great help to excellent As(V) adsorption. Load of Fe_2O_3 greatly enhanced the point of zero charge. Moreover, tubular TNTs not only inhibited dissolution of Fe_2O_3 at low pH, but also maintained good sedimentation property. The hydroxyl groups on Fe-TNTs surface played the most important role in As(V) adsorption. Electrostatic interaction followed by complexation was confirmed to be the primary adsorption mechanism by means of XPS analysis. Desorption capability and reuse performance of Fe-TNTs were also investigated, and satisfactory As(V) adsorption was further found with NaOH desorbed even after three reuse cycles.

1. Introduction

Contamination of arsenic (As) in natural waters is a worldwide problem, and As pollution attracts wide concern due to its toxicity and carcinogenicity even at low concentration [1]. Apart from natural sources of As, there are a lot of anthropogenic sources including mining, pesticide, fertilizer and coal combustion [2]. The industrial processes (such as mining) always create a highly As contaminated wastewater, which is always acidic with an extremely low pH (0.5–3) [3–5]. Typically, the As concentrations in the wastewater are in the range of 4000–15,000 mg/L (raw water) and 0.1–5 mg/L (after $Fe_2(SO_4)_3$/$FeCl_3$ addition) [5]. Furthermore, arsenate is the dominate species in natural surface water bodies and arsenite mainly exists in groundwater. Therefore, effective treatment technologies for arsenate under acidic condition are urgently needed.

In recent decades, more investigators have studied the removal of toxic As from aqueous environment and many technologies have been developed. Among the main technologies, such as oxidation [6], adsorption [7], coagulation or precipitation [8], phytoremediation [9], membrane technology [10], adsorption has been widely used in As removal area because of its advantages like simplicity in operation, low cost and higher removal efficiency [11]. Various materials such as iron oxides (goethite, lepidocrocite, hematite, magnetite), alumina, titania, and metal sulfides have been used as adsorbents [12–16]. However, most adsorbents encounter problems when used in practical applications, including slow kinetics, low efficiency, secondary pollution, difficulties in separation from water solutions and adsorbent regeneration. Moreover, only very few adsorbents can be resistant to acid environment. Furthermore, interpretation on adsorption mechanism at low pH will be of great help to As removal from industrial wastewater.

The development of nanotechnology has brought a new draw in As treatment [17–19] area. Several researchers have investigated adsorption behaviors of As on nanomaterials and reported a possible adsorption mechanism of surface complexation [20–22]. Specially, iron oxide nanoparticles such as α-F_2O_3 have been fabricated and demonstrated to show effective removal ability for As(III) and As(V) [23], whereas their low mechanical properties, especially the inefficiency of separation from water greatly inhibit their application in practical water environment [24]. Recently,

* Corresponding author at: The Key Laboratory of Water and Sediment Sciences, Ministry of Education, Department of Environmental Engineering, Peking University, Beijing 100871, China. Fax: +86 10 62756526.
E-mail address: nijinren@iee.pku.edu.cn (J. Ni).

http://dx.doi.org/10.1016/j.jcis.2014.10.036
0021-9797/

titanate nanotubes (TNTs) with small diameters and large surface area have attracted particular interests on its potential application as functional materials. TNTs can efficiently remove heavy metal ions from aqueous solutions due to their large surface area (300–400 m^2/g) [25,26] and can be easily separated from waters after application because of good aggregation and sedimentation property [27]. However, TNTs exhibit low adsorption capacity for metal anions due to the low point of zero charge (PZC). Some researches involve in Cr(VI) adsorption on modified TNTs [28,29], but rarely in As adsorption. Furthermore, although iron oxide modified titanate [30] has been synthesized, the prepare procedures are too complicated, which is not suitable for batch production. Therefore, a facile one-step synthesis method is needed in industrial application.

This study presents a novel adsorbent, iron oxide nanoparticle-grafted titanate nanotubes (Fe-TNTs), which is firstly synthesized through a facile one-step hydrothermal treatment and used for arsenate removal. Fe-TNTs successfully integrated the advantages of both Fe_2O_3 nanoparticles (abundant adsorption sites and high pH_{pzc}) [23,31] and TNTs (large surface area, acid resistance and good sedimentation) [24,26]. Adsorption behaviors of As(V) on Fe-TNTs was fully studied, and adsorption mechanism was revealed by means of XPS and FT-IR analysis. This study provides not only a new adsorbent for efficient As adsorption at acidic condition but also insight into synergetic mechanism of promising nanoparticles and TNTs.

2. Materials and methods

2.1. Materials

All chemicals used in this study were analytical grade. $FeCl_2 \cdot 4H_2O$ and $FeCl_3 \cdot 6H_2O$ were purchased from Tianjin Fuchen Chemical Co. of China. TiO_2 (P25, 80% anatase and 20% rutile; Degussa, Germany), NaOH and absolute ethanol were used to fabricate Titanate Nanotubes. $Na_2HAsO_4 \cdot 7H_2O$ (Sigma–Aldrich Co., USA) were used to prepare As(V) stock solutions by diluting with Milli-Q deionized water.

2.2. Optimization of Fe-TNTs preparation

The primary reaction factors for Fe-TNTs preparation include hydrothermal temperature, time, NaOH amount, ethanol amount and iron amount, which are shown in Table 1. Five series of experiments were conducted with different combinations of reaction temperature (130–180 °C) and reaction time from (10 to 72 h). With fixed addition amount of NaOH (11 g), ethanol (40 mL) and iron (4 mmol) in all series, the idealized combination with reaction temperature of 150 °C and reaction time of 24 h was determined in terms of the highest As(V) adsorption capacity. The optimal condition for Fe-TNTs preparation was finally determined by further evaluation with varying addition amount of NaOH (3.75–21 g), ethanol (0–55 mL) and iron (2–6 mmol). It is necessary noted that the total amount of water and ethanol was 65 mL, which implied that increasing ethanol addition would lead to decreasing water input. Hereafter, all discussions on Fe-TNTs preparation and characterization are under the optimal conditions.

2.3. Preparation of Fe-TNTs

Under the optimal conditions, Fe-TNTs was prepared as shown in Fig. S1. Firstly, 1.08 g of $FeCl_3 \cdot 6H_2O$ and 0.48 g of NaOH were mixed with 40 mL of ethanol in a beaker. After stirring for 30 min with ultrasonic oscillation, 0.6 g of P25, 21 g of NaOH and 25 mL of water were added into the beaker and then lasted for another 30 min stirring under the same condition. Further, the mixture was transferred to a 100 mL Teflon high-pressure reactor and heated at 150 °C for 24 h. Finally, when the reactor cooled to room temperature naturally, the products were washed with deionized water to pH 7 and dried at 80 °C for 6 h. TNTs used in this study were synthesized by alkaline hydrothermal method as previous studies [32]. 1.21 g Of titania and 29 g of NaOH were dispersed into 67 mL of water, and sealed in a Teflon-lined autoclave to be heated at 130 °C for 72 h. The products were washed with deionized water to neutral, and then dried at 80 °C. Synthetic method of α-Fe_2O_3 used in this study was adopted in related Ref. [33]. 2.16 g of $FeCl_3$, 0.96 g of NaOH and 80 mL of ethanol were mixed before sealed in a Teflon-lined autoclave to be heated at 150 °C for 24 h, washed with deionized water to neutral and dried at 80 °C. In this study, a new method was figured out to synthesis iron-coated titanate nanotubes.

2.4. Characterization of Fe-TNTs

The crystal structure of Fe-TNTs was measured by Powder X-ray diffraction (XRD, D/max-2400, Rigaku, Japan). The 2θ range used in the measurement was from 5° to 80°. The chemical composition of Fe-TNTs was determined by X-ray photoelectron spectroscopy (XPS, AXIS-Ultra, Kratos Analytical, UK) and Fourier Transform infrared spectroscopy (FTIR, Tensor 27, Bruker, Germany). The morphology of the materials was characterized by transmission electron microscopy (TEM, Tecnai F30, FEI, USA) operating at 300 kV. Zeta potentials of the sample under various pH conditions were measured using Zetasizer Nano ZS90 (Malvern Instruments, UK). Before the measurement of zeta potentials, 20 mg of samples were dispersed in 50 mL Milli-Q water and sonication pretreatment was processed after adjustment of the solution to different pH. Brunanuer–Emmet–Teller surface area was measured by N_2 adsorption–desorption isotherm with an Autosorb-1 Series Surface Area and Pore Analyzers (BET, ASAP 2010, Micromeritics, USA). The relative pressure (P/P_0) of 0.0654–0.2008 was used to determine the BET surface area.

Table 1
Experimental design and As(V) adsorption capacity on various Fe-TNTs prepared under different conditions.

Temperature (°C)	Time (h)	NaOH amount (g)	Ethanol amount (mL)	Iron amount (g)	Q_e (mg/g)
130	48	11	40	1.08	44.12
130	72	11	40	1.08	50.11
150	24	11	40	1.08	50.56
150	48	11	40	1.08	36.01
150	24	11	0	1.08	29.29
150	24	11	55	1.08	47.45
150	24	3.75	40	1.08	46.25
150	24	21	40	1.08	60.21
180	10	11	40	1.08	29.53
150	24	11	40	0.54	44.13
150	24	11	40	1.62	54.01

2.5. Batch adsorption experiment

Before batch adsorption experiment, effect of adsorbent dosage on removal efficiency and adsorption capacity was investigated and presented in Fig. S2. As can been seen, 0.2 g/L adsorbent dosage could reach a satisfactory removal efficiency as well as a high adsorption capacity. For the batch adsorption studies, 10 mg of Fe-TNTs were added into 50 mL As(V) solutions with concentration of 10 mg/L. Solution pH was adjusted to 1–6 using 0.1 M HCl and 0.1 M NaOH. The solutions were then shaken for 6 h (200 rpm, 25 °C). After adsorption, supernatants were centrifuged with a speed of 10,000 rpm to eliminate residual adsorbents. The solution pH after adsorption was also detected and the materials with As(V) adsorbed were collected by filtration for characterizations. For comparison, experiments on As(V) adsorption at different pH with addition of 10 mg TNTs, as well as mixture of 3 mg Fe_2O_3 and 7 mg TNTs (dosage ratio of TNTs/Fe_2O_3 in the composite material was determined by ICP-MS analysis) were also investigated respectively.

Adsorption isotherms were studied by altering initial As(V) concentration from 1 to 50 mg/L at pH 2 and the dosage of Fe-TNTs was 0.2 g/L. The adsorption kinetics were conducted at pH 2, and three different initial As(V) concentrations (5, 10, and 20 mg/L) with 0.2 g/L adsorbents were investigated. 1 mL of sample was taken out and filtered at different contact time intervals.

Furthermore, effect of coexisting anions (phosphate, sulfate, and nitrite) on arsenic adsorption was also investigated at pH 2. The molar concentration of competitive anions was varied as 1, 5 and 10 times of As(V) (10 mg/L) with the Fe-TNTs dosage of 0.2 g/L.

Concentration of As(V) was determined by atomic fluorescence spectrum (AFS, AFS-9130, Jitian, Beijing, China). The adsorption capacity (Q_e, mg/g) at equilibrium and the removal efficiency R (%) are calculated by:

$$Q_e = \frac{(C_0 - C_e)V}{m} \quad (1)$$

$$R = \frac{(C_0 - C_e)}{C_0} \times 100\% \quad (2)$$

where C_0 (mg/L) and C_e (mg/L) are initial and equilibrium concentrations of As(V), respectively; V (L) is the volume of solution, and m (g) is the mass of adsorbent added in solution. All the adsorption experiments were performed in triplicate.

2.6. As(V) desorption and reuse of Fe-TNTs

Before desorption and reuse experiment, adsorption experiment was firstly conducted at pH 2 with an initial As(V) concentration of 10 mg/L and adsorbent dosage of 0.2 g/L. When As(V) adsorption reached equilibrium, solution pH was adjusted to 10–14 and then the mixture was shaken for another 4 h. Sample was taken at equilibrium and after desorption for As(V) concentration measurement. Desorbed Fe-TNTs were obtained by centrifugation with a speed of 4000 rpm and then dried at 80 °C for 6 h. A three adsorption–desorption cycle was conducted to evaluate the adsorption performance of desorbed Fe-TNTs.

The desorption efficiency D (%) is calculated by

$$D = \frac{C_d - C_e}{C_0 - C_e} * 100\% \quad (3)$$

where C_0 (mg/L) and C_e (mg/L) are initial and equilibrium concentrations of As(V), C_d (mg/L) is concentration of As(V) after desorption.

2.7. Potentiometric titration of Fe-TNTs

To determine the amount of functional groups on Fe-TNT surface, a titration test was carried out by an automatic potentiometric titrator (AT 500N, Kyoto Electronics Manufacturing, Japan) under nitrogen stream. 10 mg Fe-TNTs was mixed with 50 mL unionized water. 0.1 M HNO_3 was used to adjust initial pH to 2.0 and then 0.1 M NaOH doses were incrementally added until the solution pH reached about 11.0. The surface charge was calculated according to the electro-neutrality theory using ProtoFit 2.1 [34].

3. Results and discussions

3.1. Optimization of Fe-TNTs preparation

As(V) adsorption capacities of various Fe-TNTs prepared under different conditions are presented in Table 1. The amount of hydroxyl group (–OH) and the microstructure of TNTs are key issues in the preparation process [35]. The prepared TNTs exhibited good tubular structure under conditions of reaction temperature 130 °C for 72 h and 150 °C for 24 h, providing more active sites for iron loading and arsenic adsorption [36]. When the hydrothermal reaction was conducted at 180 °C for 10 h, titanate nanofibers was the main products, leading to a low adsorption capability [37].

As shown in Table 1, As(V) adsorption capacity of Fe-TNTs increased with increasing NaOH concentration in the preparation process (from 3.75 g to 21 g), suggesting higher NaOH was benefited to formation of As(V) adsorption sites on the surface of adsorbent. Ethanol played two important roles in the preparation process: (1) ethanol can provide a high reaction pressure because of its high saturated vapor pressure [38]; (2) ethanol solvent at the critical state during the solvent thermal process could promote the thermal decomposition of $Fe(OH)_3$ [33]. Without addition of ethanol, TiO_2 (P25) would not convert into titanate well and $Fe(OH)_3$ could not decompose, resulting in low adsorption capacity of synthesized adsorbent. Iron amount in preparation process would affect the final adsorption capacity of synthesized material, since iron atoms in iron oxide could afford more hydroxyl groups than titanium in TNTs. Addition of 1.08 g iron would be satisfied since higher amount did not increase As(V) adsorption capacity significantly.

Therefore, the optimal reaction condition for Fe-TNTs preparation was the 150 °C of hydrothermal temperature, 24 h of reaction time, 11 g of NaOH, 25 mL of ethanol and 1.08 g of iron addition. It was noteworthy that the proposed method could also be useful to transition of other metal elements into TNTs.

3.2. Characteristics of Fe-TNTs

Fig. 1 shows TEM images of TNTs and Fe-TNTs as well as HRTEM images of Fe-TNTs. Both nanomaterials exhibited structures of hollow and open-ended tubes, but Fe-TNTs presented rougher nanotube surface. The inner and outer diameter of Fe-TNTs was ca. 8 nm and ca. 11 nm, respectively. Fe_2O_3 nanoparticles were attached on Fe-TNTs, which could also be verified by EDS analysis. HRTEM clearly shows the interlayer distance of TNTs was about 0.78 nm [25] and the lattice distance of attached nanoparticles was 0.25 nm, which were ascribed to (110) plane of iron oxide (JCPD standards No. 24-0072). The TEM and HRTEM results showed that Fe_2O_3 nanoparticles (ca. 5.1 nm) are bonded to surface of TNTs [39].

The XRD patterns of TNTs, Fe-TNTs (with 2 mmol iron addition), Fe-TNTs (with 4 mmol iron addition) and physic mixture of TNTs and Fe_2O_3 (Fig. 2) demonstrated some similar peaks at $2\theta \approx 10°$, 24°, 28° and 48°, which were respectively assigned to (200), (110), (211) and (020) planes of TNTs [40]. The peak at approxi-

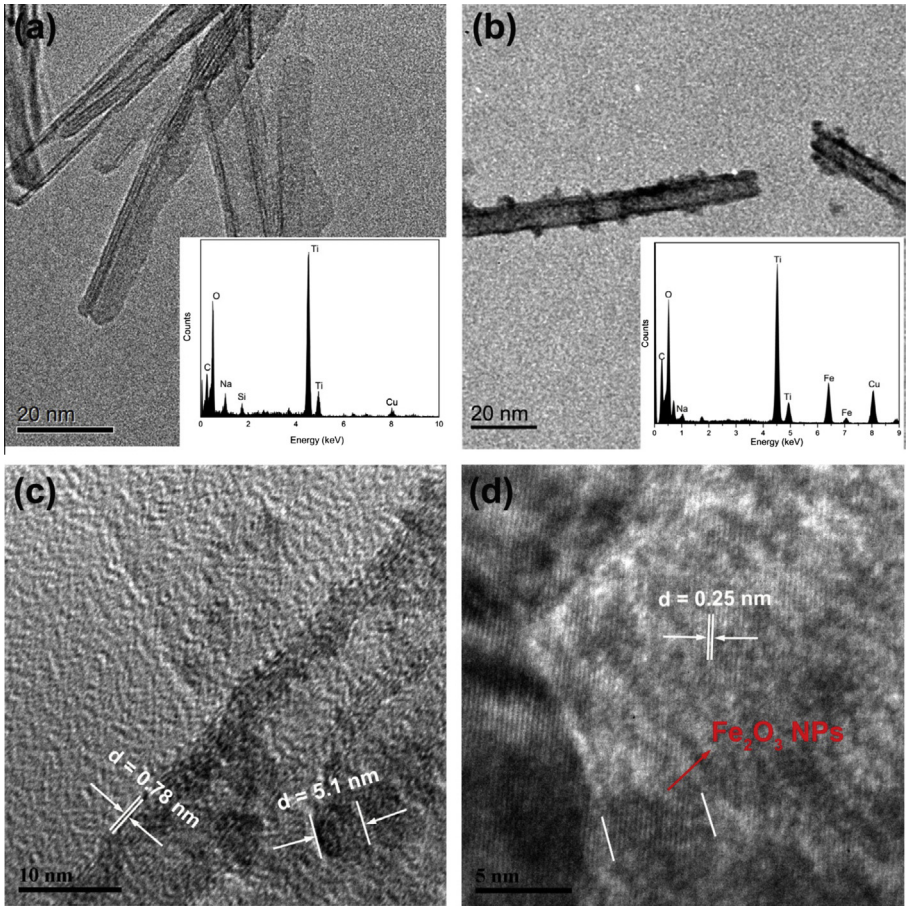

Fig. 1. TEM images of TNTs (a) and Fe-TNTs (b). HRTEM images of tubular structure (c) and lattice distance of Fe_2O_3 (d).

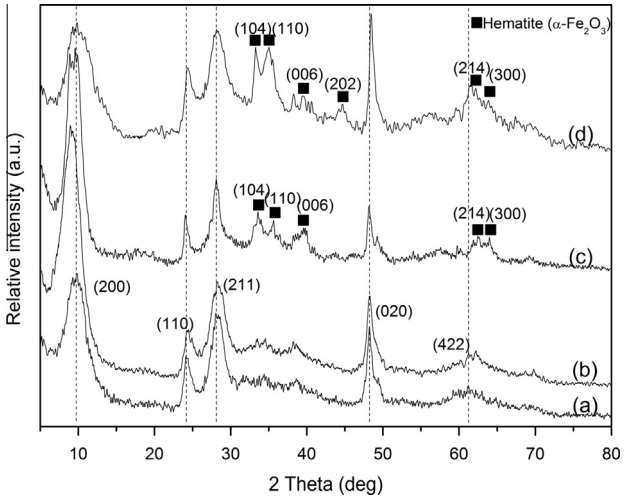

Fig. 2. XRD patterns of TNTs (a), Fe-TNTs with 2 mmol iron addition (b), Fe-TNTs with 4 mmol iron addition (c), and physic mixture of TNTs and Fe_2O_3 (d).

mate 10° decreased from 9.86° to 9.59°, indicating an increase of interlayer space of TNTs possibly due to introduction of Fe_2O_3. In Fig. 2b, the peaks of Fe-TNTs (with 2 mmol iron addition) presented almost the same as that of TNTs, indicating that iron ions had entered into titanate nanotube crystalline lattices and had been incorporated into TNTs [41,42]. For Fe-TNTs with 4 mmol iron addition (Fig. 2c), the new peaks at $2\theta = 33.58°$, 35.62°, 40.02°, 44.68°, 62.46°, and 63.98° were consistent with (104), (110), (006), (202), (214), and (300) planes of α-Fe_2O_3 phases (JCPD standards No. 24-0072), indicating separate phase of Fe_2O_3 existed apart from the incorporated iron ions. Moreover, the peaks of α-Fe_2O_3 phases in Fe-TNTs with 4 mmol iron addition were much weaker than that in physic mixture of TNTs and Fe_2O_3 (Fig. 2d), which could be ascribed the incorporation of iron into TNTs. Therefore, there are two main forms in the grafting procedure: one is incorporation of iron and the other one is graft of iron oxide nanoparticles.

To further verify the iron incorporation into TNTs, Raman spectra of TNTs and Fe-TNTs with 2 mmol iron addition are presented in Fig. S4. Both Raman peaks are similar. The peak at 901 cm^{-1} was attributed to four-coordinate Ti–O stretching vibration [40]. The peaks at 271 cm^{-1} and 660 cm^{-1} were suggested to be ascribed to Na–O–Ti [43]. The peak at 440 cm^{-1} was due to Ti–O bending and stretching vibration involving six-coordinated titanium and three-coordinated oxygen [44]. No separate peaks of Fe_2O_3 are observed, indicating that there is a strong coupling between Fe_2O_3 and TNTs, and Fe_2O_3 was incorporated into TNTs [39].

The physicochemical properties of Fe-TNTs are presented in Table 2. The specific surface area and pore volume of Fe-TNTs were 162.8 m^2/g and 0.3794 cm^3/g respectively, which were less than that of TNTs due to inevitable block of pores by iron oxide loading. The point of zero charge for Fe-TNTs was 5.49 (Fig. S2), which was much higher than that of TNTs (3.06). Therefore, Fe-TNTs were positively charged in a wider pH range and it was more favorable for As(V) adsorption. The amount of hydroxyl groups on the surface of TNTs and Fe-TNTs was about 2.23 mmol/g and 2.46 mmol/g. More hydroxyl groups were observed on the surface of Fe-TNTs than TNTs, which could be helpful for arsenate adsorption.

Table 2
Physicochemical properties of TNTs and Fe-TNTs.

Parameters	TNTs [24]	Fe-TNTs
BET surface area	240.2 m^2/g	162.8 m^2/g
V_{BJH}	0.7940 cm^3/g	0.3794 cm^3/g
Point of zero charge	3.07	5.49
Hydroxyl groups	2.23 mmol/g	2.46 mmol/g
Atomic percentage content	O 1s 65.82%	O 1s 62.06%
	Ti 2p 22.95%	Ti 2p 18.78%
		Fe 2p 8.01%
	Na 1s 11.23%	Na 1s 11.15%

3.3. Adsorption behaviors of As(V) on Fe-TNTs

3.3.1. Adsorption kinetics

Pseudo-first and pseudo-second order kinetic models are introduced to describe the adsorption kinetic data, which are expressed as [28]:

$$\mathrm{Ln}\left(1-\frac{Q_t}{Q_e}\right)=-k_1 t \tag{4}$$

$$\frac{t}{Q_t}=\frac{1}{k_2 Q_e^2}+\frac{1}{Q_e}t \tag{5}$$

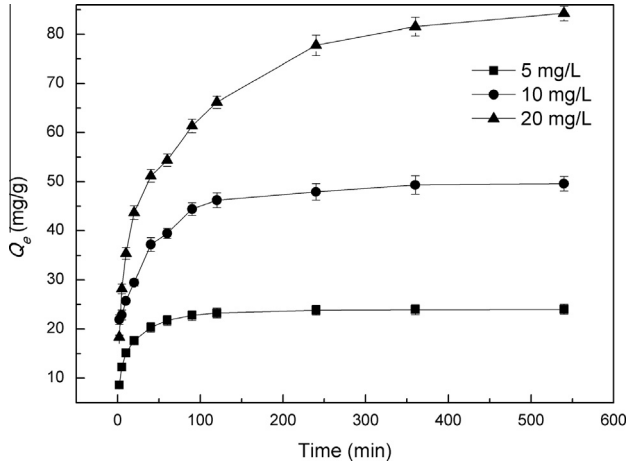

Fig. 3. Adsorption kinetics of As(V) on Fe-TNTs (adsorbent dosage = 0.2 g/L, T = 25 °C, pH = 2).

where Q_e (mg/g) and Q_t (mg/g) are the adsorbed capacity of As(V) at equilibrium and time t (min); k_1 (min^{-1}) and k_2 (mg/(g min)) are the pseudo-first and pseudo-second order rate constant, respectively.

Adsorption kinetics results are presented in Fig. 3. There was a quick uptake of As(V) in the first 120 min, and then reached equilibrium within 300 min when initial As(V) concentration was 5 or 10 mg/L. Relative parameters for kinetics models are shown in Table 3. It was found that the data fit pseudo-second order model well ($R^2 > 0.995$). Moreover, the calculated Q_e from the model showed good agreement with the experimental results. The kinetic results suggested that chemisorption might be the rate-limiting step for As(V) adsorption on Fe-TNTs [45]. In addition, the pseudo-second-order rate constant reflects the adsorption rate of adsorbate onto adsorbent [45]. It was found the pseudo-second-order rate constant decreased as the increasing As(V) initial concentration, it was due to abundant As(V) anions competed for adsorption sites located on Fe-TNTs at high As(V) concentration and resulted in low adsorption rate (see Fig. 3).

3.3.2. Adsorption isotherms

Adsorption isotherms of As(V) onto Fe-TNTs are tested with Langmuir, two-site Langmuir and Freundlich models, respectively [46]:

$$Q_e=\frac{Q_m b C_e}{1+bC_e} \tag{6}$$

$$Q_e=\frac{Q_1 b_1 C_e}{1+b_1 C_e}+\frac{Q_2 b_2 C_e}{1+b_2 C_e} \tag{7}$$

$$Q_e=K_F C_e^{1/n} \tag{8}$$

where Q_m (mg/g) is the maximum adsorption capacity (mg/g) determined from Langmuir model, and b (L/mg) is the affinity coefficients of adsorption site on the adsorbents. The two-site Langmuir isotherms fit the adsorption data well when there are two types of adsorption sites with different binding energies on the adsorbents. [47] Q_1 (mg/g) and Q_2 (mg/g), b_1 (L/mg) and b_2 (L/mg) in Eq. (4) are the maximum adsorption capacity and the affinity coefficients of sites 1 and 2 on the adsorbents, respectively. The total maximum adsorption capacity can be obtained by adding Q_1 with Q_2. K_F (mg/g) and n are adsorption affinity coefficient and heterogeneity factor indicating the adsorption intensity of the adsorbent.

Table 3
Parameters of kinetic models for As(V) adsorption on Fe-TNTs.

C_0 (mg/L)	Kinetic models					
	Pseudo-first			Pseudo-second		
	Q_e (mg/g)	k_1 (g/(mg min)	R^2	Q_e (mg/g)	k_2 (g/(mg min)	R^2
5	22.39	0.133	0.852	24.34	0.0139	0.999
10	45.21	0.123	0.673	50.21	0.00446	0.999
20	75.04	0.0489	0.757	90.66	0.000947	0.996

Table 4
Parameters of isotherm models for As(V) adsorption on TNTs and Fe-TNTs.

Adsorbent	Isotherm models										
	Langmuir			Two-site					Freundlich		
	b (L/mg)	Q_m (mg/g)	R^2	Q_1 (mg/g)	Q_2 (mg/g)	b_1 (L/mg)	b_2 (L/mg)	R^2	K_F (mg/g)	n	R^2
Fe-TNTs	4.55	80.67	0.66	37.93	53.03	11.40	0.04	0.96	36.41	6.02	0.94
TNTs	10.04	32.40	0.99	–	–	–	–	–	19.63	8.54	0.83

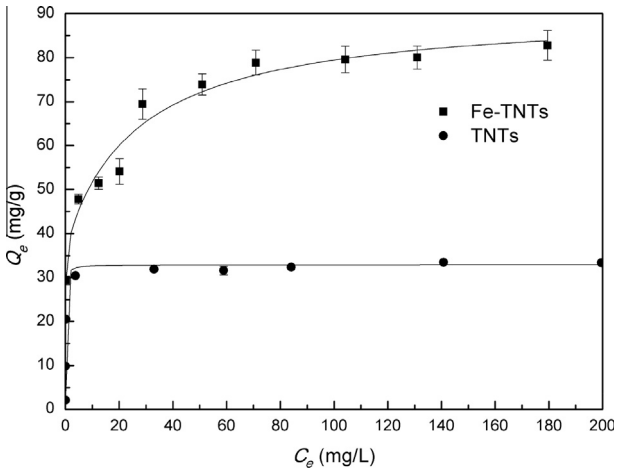

Fig. 4. Adsorption isotherm for the adsorption of As(V) on TNTs and Fe-TNTs (adsorbent dosage = 0.2 g/L, T = 25 °C, pH = 2).

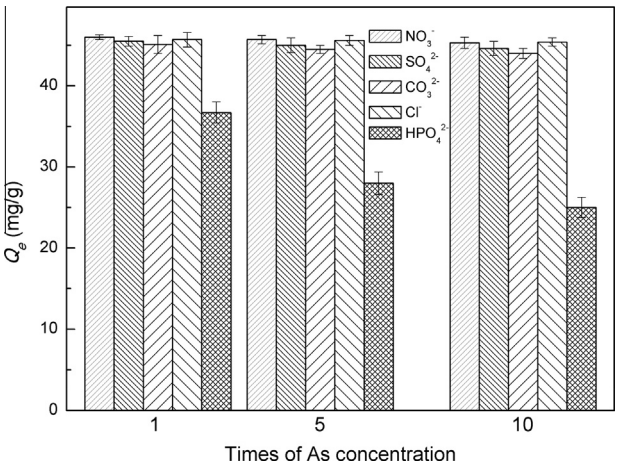

Fig. 5. Effect of coexisting anions on adsorption of As(V) on Fe-TNTs (adsorbent dosage = 0.2 g/L, T = 25 °C, pH = 2).

Table 4 shows the parameters for different isotherm models, and Fig. 4 presents the adsorption isotherm of As(V) on TNTs and Fe-TNTs. Adsorption of As(V) onto TNTs was only analyzed by Langmuir and Freundlich model due to their single adsorption sites (–OH/Na), while the adsorption by Fe-TNTs was specially investigated by two-site Langmuir model because of the two kinds of adsorption sites (TNTs and Fe_2O_3) located. It could be found that the two-site Langmuir model fit the data well (R^2 = 0.96), indicating two types of adsorption sites took effect when As(V) was adsorbed onto Fe-TNTs. TNTs and α-Fe_2O_3 were the two materials that afforded adsorption sites. The adsorption capacity of one site (Q_1 = 37.93 mg/g) was similar to that of TNTs (Q_m = 32.40 mg/g), which should be ascribed to adsorption site of TNTs. The other site with capacity of 53.03 mg/g (Q_2) should be assigned to α-Fe_2O_3. Therefore, the composite Fe-TNTs made full use of adsorption sites of both TNTs and α-Fe_2O_3. It was noteworthy that adsorption capacity of TNTs on Fe-TNTs (Q_1 = 37.93 mg/g) was larger than that of single TNTs (Q_m = 32.40 mg/g), due to enhancement of pH_{pzc} for Fe-TNTs. Fe-TNTs with more positive charges at pH 2–6 could more easily attracted arsenate anions than TNTs. The adsorption capacity and removal efficiency were 24.16 mg/g and 99.8% when the As(V) equilibrium concentration was 10 ppb, indicating excellent removal efficiency of As(V) by Fe-TNTs. More importantly, the maximum adsorption capacity of Fe-TNTs was as high as 90.96 mg/g, which was almost 3 times of TNTs, indicating that loading of α-Fe_2O_3 onto TNTs was an effective method for improving As(V) adsorption performance.

For comparison, arsenate removal capacities of both TNTs and Fe-TNTs were listed in Table 5, together with those of other commercially available materials and reported materials in literatures. Among them, Hombikat UV100 TiO_2 and Degussa P25 TiO_2 had lower capacity (4.6–22.5 mg/g at pH 4.0) than Fe-TNTs. Even for iron oxide-loaded melted slag, its arsenate removal capacity (18.8–78.5 mg/g at pH 2.5) was still lower than Fe-TNTs' (90.96 mg/g) under similar conditions.

3.3.3. Effect of coexisting anions

Coexisting inorganic anions always influence As(V) adsorption onto adsorbents in the practical wastewaters. In this study, NO_3^-, SO_4^{2-}, CO_3^{2-}, Cl^- and HPO_4^{2-} were chosen as representative anions to investigate the competitive adsorption behaviors. As presented in Fig. 5, NO_3^-, SO_4^{2-}, $CO_3^{2-}$and Cl^- had little effect on adsorption of As(V) onto Fe-TNTs. The adsorption capacity of As(V) was still up to 45.3, 44.6, 44.1, 45.4 mg/g even when the concentration of NO_3^-, SO_4^{2-}, $CO_3^{2-}$and Cl^- was 10 times larger than As(V), which were a little lower than that in the absence of these anions. However, coexisting HPO_4^{2-} greatly inhibited the adsorption of As(V), and the adsorption capacity reduced to 25.0 mg/g when concentration of HPO_4^{2-} was 10 times of As(V). The similar charge property and steric configuration of P in HPO_4^{2-} with As was the primary reason for inhibition, and the anions competed for the adsorption sites with arsenate [31].

3.4. Synergistic effect

As(V) adsorption capacity by different adsorbents at pH 1–6 are presented in Figs. 6 and S3 shows species distribution of arsenate as a function of pH. H_3AsO_4 was the dominate species at pH < 2 and anions of As(V) were observed at pH > 2. As(V) adsorption capacity of all the three adsorbents decreased as the pH increased from 2 to 6 due to more and more negative surface charge. The electrostatic interaction between As(V) anions and positively charged materials played an important role in adsorption process. At pH 2–3, the surface charge of the adsorbent was positive and the dominate species of As(V) was $H_2AsO_4^-$, which implied that As(V) could easily approach the surface of adsorbent and then form

Table 5
Comparison of arsenate removal capacity of various Fe or Ti based adsorbents.

Adsorbent	pH	Concentration/range (mg/L)	Capacity (mg/g)	References
Hombikat UV100 TiO_2	4.0	~37.5	~22.5	[48]
Degussa P25 TiO_2	4.0	~37.5	~4.6	[48]
Fe-Ti oxide	7.0	5.0–250	14.0	[49]
TNTs	3.0	1.0–200	32.4	This study
Iron oxide-loaded melted slag	2.5	20–300	18.8–78.5	[50]
Iron oxide coated cement	~7	0.5–10.0	6.43	[51]
Iron oxide grafted TNTs	3.0	1.0–200	90.96	This study

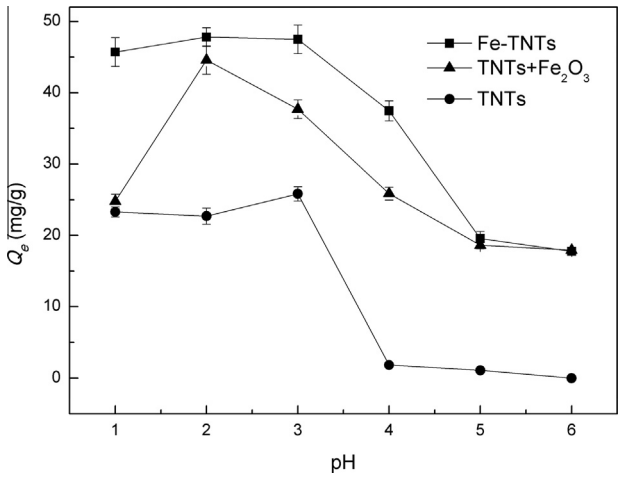

Fig. 6. Adsorption capacity of As(V) on TNTs, mixed materials of TNTs and Fe_2O_3 (TNTs + Fe_2O_3), and Fe-TNTs at different pH. (Initial As(V) concentration = 10 mg/L, adsorbent dose = 0.2 g/L, T = 25 °C).

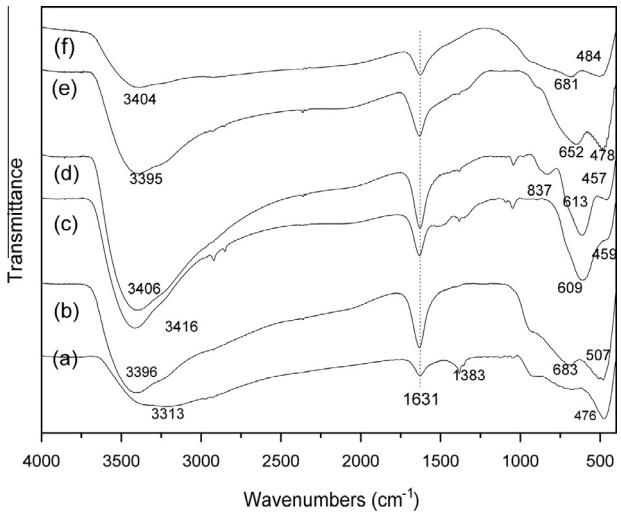

Fig. 7. FTIR spectra of TNTs (a and b), Fe_2O_3 (c and d) and Fe-TNTs (e and f) before and after As(V) adsorption.

complex with –OH of Fe-TNTs. The mixed material (TNTs + Fe_2O_3) presented a higher removal efficiency than TNTs themselves but lower than Fe-TNTs in all pH ranges, which demonstrated synergistic effect for As(V) adsorption occurred when iron oxide loaded onto TNTs. In other words, the TNTs after grafting with Fe_2O_3 would have more surface positive charges at pH 2–5 than original TNTs and would provide more access to arsenate anions thus higher possibility of complexation with arsenate anions. However, Fe-TNTs at pH 5–6 was almost no charge to provide for complexation and not able to enhance adsorption capability. This implied that the electrostatic interaction between As(V) anions and positively charged materials played an important role in the adsorption process. The adsorption capacity of mixed material reduced at pH 1, due to dissolve of iron oxide (Table S1). However, with iron oxide loading on TNTs, its dissolving into solutions could be restricted at pH < 2 (Table S1), which is of high potential to practical applications in strongly acidic wastewater treatment. Moreover, strong bonding between Fe_2O_3 and TNTs strengthened Fe-TNTs' acid-resistant capability and restricted dissolution of Fe_2O_3 on it at extreme acidic condition. With 0.2 g/L Fe-TNTs, an initial As(V) 10 mg/L in aqueous water could be reduced to 0.5 mg/L as required by China's discharge standard. Besides, Fe-TNTs presented excellent sedimentation property (Fig. S7), which made separation of adsorbents from solutions much easier.

Comparing with the physical mixture material, the graft of iron oxide onto TNTs apparently increased TNTs' surface charge and consequently enhanced Fe-TNTs' As adsorption capacity. In particular, TNTs could protect Fe_2O_3 from dissolving into solution at pH < 2 because of the incorporation of iron. Moreover, Fe-TNTs also presented better sedimentation property than Fe_2O_3, which is helpful in separation of adsorbents.

3.5. As(V) adsorption mechanism of Fe-TNTs

FTIR spectra of TNTs, Fe_2O_3 and Fe-TNTs before and after As(V) adsorption are depicted in Fig. 7. Obviously, all the FTIR spectra showed H–O–H stretching (3300–3400 cm^{-1}) and bending (1631 cm^{-1}) vibration of water [52]. The peak at 476 cm^{-1} corresponding to Ti–O–Ti band (Fig. 7a) [26] did not shift a lot after iron loaded, whereas a new peak at 652 cm^{-1} (Fig. 7e) related to Fe–O band appeared [53]. Compared Fe_2O_3 with Fe-TNTs, the peak at 609 cm^{-1} (Fig. 7c) which represented Fe–O in iron oxide [53] shifted to 652 cm^{-1} (Fig. 7e) due to interference of titanium atoms.

For TNTs with As(V) adsorbed, a new peak at 683 cm^{-1} appeared (Fig. 7b), due to the formation of Ti–O–As bond. And the peak at 1383 cm^{-1} corresponding to O–Na band disappeared [28], indicating that Na atom was replaced by other atoms (H or As). The peak at 476 cm^{-1} corresponding to Ti–O–Ti band shifted to 507 cm^{-1}, suggesting the change of Ti–O groups after the adsorption. Moreover, the new peak at 837 cm^{-1} (Fig. 7d) was corresponded to As–O stretching vibration [54], which indicated As(V) was adsorbed onto the iron oxide successfully. For Fe-TNTs with As(V) adsorbed (Fig. 7f), the peak at 652 cm^{-1} attributed to Fe–O groups shifted to 681 cm^{-1} after adsorption, suggesting metal–oxygen (M–O) groups played an important role in the adsorption process. It should be pointed out that the As–O band at approximate 800 cm^{-1} after As(V) adsorption was not clearly observed because of the broad overlapping peaks in their region [55].

Fig. 8 presents XPS spectra of Fe-TNTs before and after As(V) adsorption. As shown in the survey spectra (Fig. 8a), the peak of Na 1s disappeared after adsorption, suggesting Na^+ was replaced by H^+ or arsenate ions at low pH (2). Besides, As 3d peak appeared after adsorption, indicating As(V) was adsorbed onto the materials. For high resolution of O 1s (Fig. 8b), oxygen was composed of overlapped peaks positioned at 529.85 and 531.13 eV, which was assigned to metal oxide (M–O) and hydroxyl bonded to metal (M–OH), respectively [35]. After adsorption, changes of peak position and composition percent of M–O (530.14 eV) and M–OH were observed due to interaction between surface –OH and As(V).

For the high resolution spectra of Ti 2p, the peak at 458.1 and 464.0 eV was ascribed to Ti $2p_{3/2}$ and Ti $2p_{1/2}$, respectively (Fig. 8c) [24]. Both peaks of Ti shifted after adsorption, indicating that the hydroxyl groups bonded to Ti may involve in As(V) adsorption. Photoelectron peaks at 711 and 725 eV in Fig. 8d correspond to the binding energies of 2p3/2 and 2p1/2 of oxidized iron (Fe(III)) [56], and the peaks of Fe shifted, indicating that the hydroxyl groups bonded to Fe may involve in As(V) adsorption. Therefore, both the hydroxyl groups bonded to Ti and Fe involved in As(V) adsorption, indicating these two kinds of adsorption sites on TNTs and Fe_2O_3 took effect as described by the two-site Langmuir isotherm. Fig. 8e presents the As 3d spectra, the new peak at 45.6 eV after adsorption should be attributed to As(V) [24], demonstrating a successful adsorption of As(V) on the adsorbent surface.

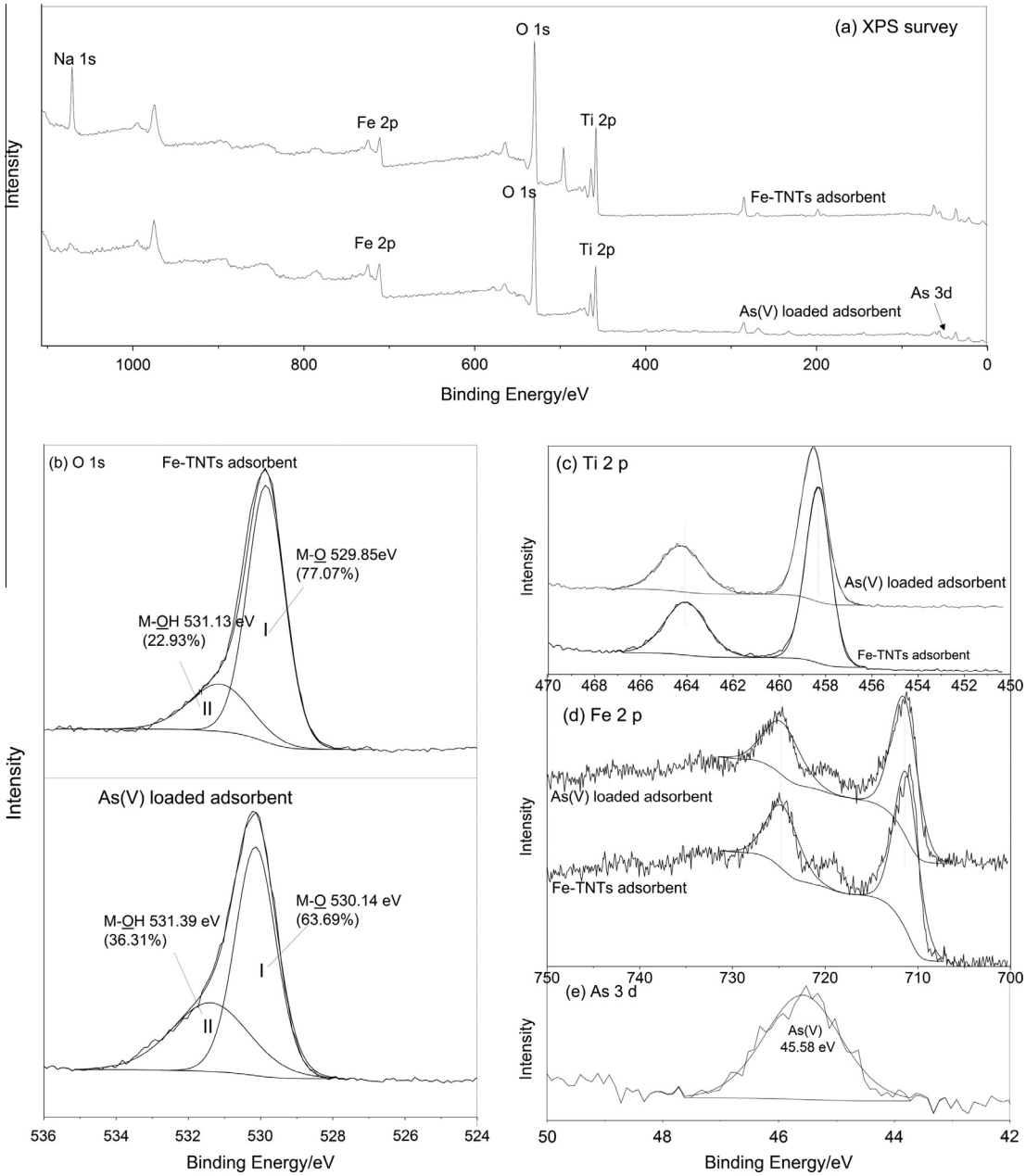

Fig. 8. XPS spectra of (a) survey and high resolution of (b) O 1s, (c) Ti 2p, (d) Fe 2p, (d) As 3d for Fe-TNTs before and after As(V) adsorption.

In short, the hydroxyl groups on Fe-TNTs surface played the most important role in As(V) adsorption, and the adsorption mechanism was ligand exchange as illustrated in Fig. 9. Moreover, the electrostatic interaction between As(V) anions and positively charged materials could not be ignored. Electrostatic interaction followed by complex process is confirmed to be the primary adsorption mechanism.

3.6. Desorption and adsorbent reuse

Adsorbent reuse is always important for cost-effective adsorption. In this study, NaOH solution was used to desorb As(V) with less damage of tubular structure of Fe-TNTs. In Fig. 10, a general increasing trend of As(V) desorption efficiency was observed with increase of OH^- concentration (pH from 10 to 14). Higher desorption efficiency (82–96%) could be expected at pH 12–14, which was benefited to adsorbent reuse. The adsorbent was then reused to remove As(V) from solution after desorbed with NaOH at pH 13. Even after three adsorption–desorption cycles, As(V) adsorption capacity of Fe-TNTs was as high as 72 mg/g, only 20% less than that of fresh Fe-TNTs. Fe and Ti concentrations were measured by ICP-MS after regeneration experiments, but almost no Fe or Ti element was detected, which indicated very good physical and chemical stability of this material in basic medium. Besides, excellent sedimentation property of Fe-TNTs made separation of the adsorbents from solutions much easier (Fig. S7).

Overall, Fe-TNTs is of great potential in practical applications because of its high As(V) adsorption efficiency, good sedimentation property, easy desorption and satisfactory performance in reuse. More importantly, Fe-TNTs could be a wonderful substitute for Fe_2O_3 in the application of As contaminated industrial wastewater in strongly acidic condition due to its acid resistance.

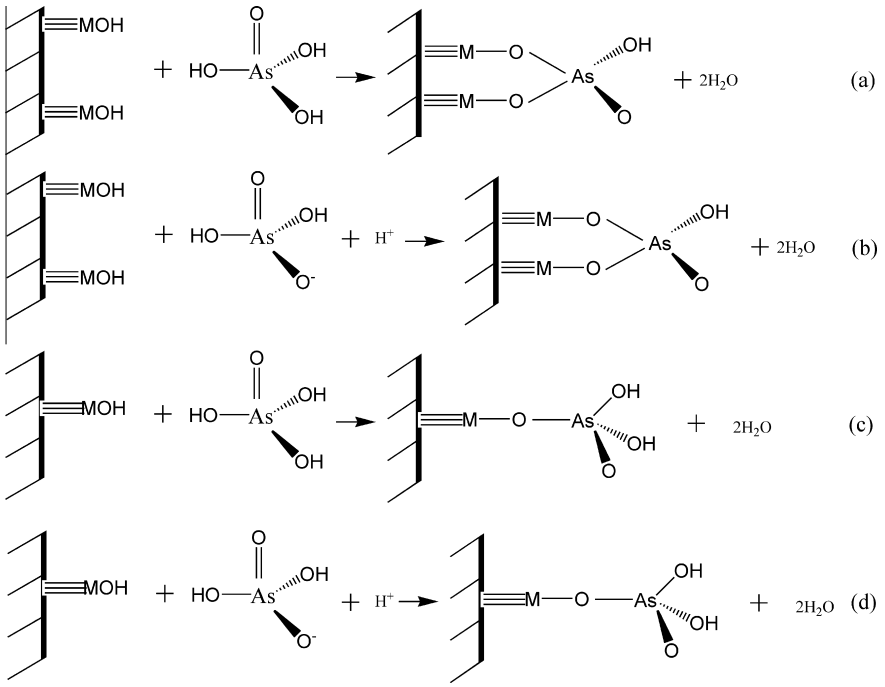

Fig. 9. Schematic diagram for the formation of As(V) complexes on the surface of Fe-TNTs (M represents Fe or Ti) at pH 2.

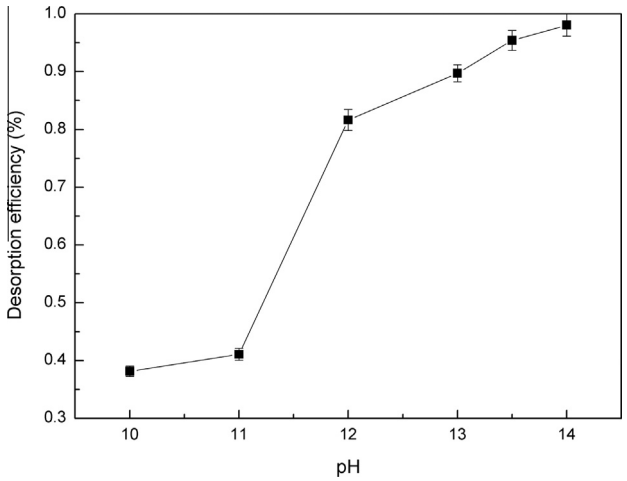

Fig. 10. Desorption efficiency of As(V) from Fe-TNTs under different pH.

4. Conclusions

An acid-resistant adsorbent Fe-TNTs was directly synthesized by one-step water–ethanol hydrothermal method with successful grafting of iron oxide nanoparticles onto TNTs. Fe-TNTs was convinced as a composite phase of TNTs and α-Fe_2O_3 by TEM and XRD analysis. As(V) adsorption capacity of Fe-TNTs was as high as 3 times of original TNTs according to the two-site Langmuir model, and As(V) could be efficiently removed from 10 to 0.5 mg/L at low pH (2–3). Synergy of Fe_2O_3 and TNTs for As(V) adsorption was essential to such an excellent adsorption property, which could be further interpreted with the increased point of zero charge by Fe_2O_3 grafting. Coexisting NO_3^-, SO_4^{2-}, CO_3^{2-} and Cl^- had insignificant influence on As(V) adsorption, but HPO_3^{2-} inhibited adsorption. XPS analysis revealed that the adsorption mechanism was dominated by hydroxyl groups on Fe-TNTs surface in the form of complexation. Moreover, Fe-TNTs performed good As(V) removal efficiency after desorbed by NaOH solution even after three reuse cycles. Overall, Fe-TNTs is of great potential in As removal owing to its apparent advantages such as large adsorption capacity, good sedimentation property, easy desorption and satisfactory performance in reuse as well as its acid resistance which is of particular use to arsenate wastewater treatment at acidic conditions.

Acknowledgments

Financial support is from open fund of State Key Laboratory of Soil Erosion and Dryland Farming on the Loess Plateau (K318009902-1428). Support from Collaborative Innovation Center for Regional Environmental Quality is also acknowledged.

Appendix A. Supplementary material

Supplementary data associated with this article can be found, in the online version, at http://dx.doi.org/10.1016/j.jcis.2014.10.036.

References

[1] M.F. Hughes, Toxicol. Lett. 133 (2002) 1.
[2] J.F. Ferguson, J. Gavis, Water Res. 6 (1972) 1259.
[3] K.L. Allende, T.D. Fletcher, G. Sun, Chem. Eng. J. 179 (2012) 119.
[4] J.H. Kyle, P.L. Breuer, K.G. Bunney, R. Pleysier, Hydrometallurgy 111–112 (2012) 10.
[5] P. Nunez, H.K. Hansen, S. Aguirre, C. Maureira, Sep. Purif. Technol. 79 (2011) 285.
[6] M.C. Dodd, N.D. Vu, A. Ammann, V.C. Le, R. Kissner, H.V. Pham, T.H. Cao, M. Berg, U. Von Gunten, Environ. Sci. Technol. 40 (2006) 3285.
[7] Y.H. Kim, C.M. Kim, I.H. Choi, S. Rengaraj, J.H. Yi, Environ. Sci. Technol. 38 (2004) 924.
[8] S.R. Wickramasinghe, B.B. Han, J. Zimbron, Z. Shen, M.N. Karim, Desalination 169 (2004) 231.
[9] N. Singh, L.Q. Ma, Environ. Pollut. 141 (2006) 238.
[10] M.D. Ballinas, E.R. De San Miguel, M.T.D. Rodriguez, O. Silva, M. Munoz, J. De Gyves, Environ. Sci. Technol. 38 (2004) 886.
[11] C. Nieto-Delgado, J. Rene Rangel-Mendez, Water Res. 46 (2012) 2973.
[12] S. Dixit, J.G. Hering, Chem. Geol. 228 (2006) 6.

[13] G. Ona-Nguema, G. Morin, Y. Wang, F. Juillot, M. Abdelmoula, C. Ruby, F. Guyot, G. Calas, G.E. Brown Jr., Geochim. Cosmochim. Acta 73 (2009) A973.
[14] A.D. Redman, D.L. Macalady, D. Ahmann, Environ. Sci. Technol. 36 (2002) 2889.
[15] H. Guo, D. Stueben, Z. Berner, Appl. Geochem. 22 (2007) 1039.
[16] J. Gimenez, M. Martinez, J. de Pablo, M. Rovira, L. Duro, J. Hazard. Mater. 141 (2007) 575.
[17] M.E. Pena, G.P. Korfiatis, M. Patel, L. Lippincott, X.G. Meng, Water Res. 39 (2005) 2327.
[18] S. Bang, M. Patel, L. Lippincott, X. Meng, Chemosphere 60 (2005) 389.
[19] M. Pena, X.G. Meng, G.P. Korfiatis, C.Y. Jing, Environ. Sci. Technol. 40 (2006) 1257.
[20] D.S. Han, A. Abdel-Wahab, B. Batchelor, J. Colloid Interface Sci. 348 (2010) 591.
[21] R. Chen, C. Zhi, H. Yang, Y. Bando, Z. Zhang, N. Sugiur, D. Golberg, J. Colloid Interface Sci. 359 (2011) 261.
[22] T. Tuutijarvi, J. Lu, M. Sillanpaa, G. Chen, J. Hazard. Mater. 166 (2009) 1415.
[23] W. Tang, Q. Li, S. Gao, J.K. Shang, J. Hazard. Mater. 192 (2011) 131.
[24] H.Y. Niu, J.M. Wang, Y.L. Shi, Y.Q. Cai, F.S. Wei, Micropor. Mesopor. Mater. 122 (2009) 28.
[25] W. Liu, T. Wang, A.G.L. Borthwick, Y. Wang, X. Yin, X. Li, J. Ni, Sci. Total Environ. 456–457 (2013) 171.
[26] T. Wang, W. Liu, L. Xiong, N. Xu, J. Ni, Chem. Eng. J. 215 (2013) 366.
[27] W. Liu, W. Sun, A.G.L. Borthwick, J. Ni, Colloids Surf., A 434 (2013) 319.
[28] G. Niu, W. Liu, T. Wang, J. Ni, J. Colloid Interface Sci. 401 (2013) 133.
[29] L. Wang, W. Liu, T. Wang, J. Ni, Chem. Eng. J. 225 (2013) 153.
[30] A.L. Papa, L. Maurizi, D. Vandroux, P. Walker, N. Millot, J. Phys. Chem. C 115 (2011) 19012.
[31] S. Lin, D. Lu, Z. Liu, Chem. Eng. J. 211 (2012) 46.
[32] Q. Chen, W.Z. Zhou, G.H. Du, L.M. Peng, Adv. Mater. 14 (2002) 1208.
[33] W. Tang, Q. Li, C. Li, S. Gao, J.K. Shang, J. Nanopart. Res. 13 (2010) 2641.
[34] S. Schiewer, A. Balaria, Chem. Eng. J. 146 (2009) 211.
[35] Y. Zhang, M. Yang, X.M. Dou, H. He, D.S. Wang, Environ. Sci. Technol. 39 (2005) 7246.
[36] D.V. Bavykin, Eur. J. Inorg. Chem. (2009) 977.
[37] D.V. Bavykin, V.N. Parmon, A.A. Lapkin, F.C. Walsh, J. Mater. Chem. 14 (2004) 3370.
[38] X. Shen, J. Zhang, B. Tian, J. Mater. Sci. 47 (2012) 3855.
[39] H. An, J. Li, J. Zhou, K. Li, B. Zhu, W. Huang, J. Mater. Chem. 20 (2010) 603.
[40] X. Sun, Y. Li, Chem. – Eur. J. 9 (2003) 2229.
[41] X. Wei, H. Wang, G. Zhu, J. Chen, L. Zhu, Ceram. Int. 39 (2013) 4009.
[42] X. Ding, X.G. Xu, Q. Chen, L.M. Peng, Nanotechnology 17 (2006) 5423.
[43] H.M. Kim, F. Miyaji, T. Kokubo, T. Nakamura, J. Mater. Sci. – Mater. Med. 8 (1997) 341.
[44] R.Z. Ma, K. Fukuda, T. Sasaki, M. Osada, Y. Bando, J. Phys. Chem. B 109 (2005) 6210.
[45] X. Xin, Q. Wei, J. Yang, L. Yan, R. Feng, G. Chen, B. Du, H. Li, Chem. Eng. J. 184 (2012) 132.
[46] Y. Jin, F. Liu, M. Tong, Y. Hou, J. Hazard. Mater. 227 (2012) 461.
[47] G. Birlik, G. Demirel, M. Cakmak, T. Caykara, Surf. Sci. 601 (2007) 3760.
[48] P.K. Dutta, A.K. Ray, V.K. Sharma, F.J. Millero, J. Colloid Interface Sci. 278 (2004) 270.
[49] K. Gupta, U.C. Ghosh, J. Hazard. Mater. 161 (2009) 884.
[50] F.S. Zhang, H. Itoh, Chemosphere 60 (2005) 319.
[51] S. Kundu, A.K. Gupta, Sep. Purif. Technol. 51 (2006) 165.
[52] G. Zhang, J. Qu, H. Liu, R. Liu, R. Wu, Water Res. 41 (2007) 1921.
[53] C.T. Wang, S.H. Ro, Mater. Chem. Phys. 101 (2007) 41.
[54] S. Goldberg, C.T. Johnston, J. Colloid Interface Sci. 234 (2001) 204.
[55] L. Zhijian, D. Shubo, Y. Gang, H. Jun, V.C. Lim, Chem. Eng. J. 161 (2010) 106.
[56] X.Q. Li, W.X. Zhang, J. Phys. Chem. C 111 (2007) 6939.